# Impact of spatial variability of shear wave velocity on the lagged coherency of synthetic surface ground motions

E. El Haber, C. Cornou, D. Jongmans, Fernando Lopez-caballero, D. Youssef Abdelmassih, T. Al-Bittar

# Impact of spatial variability of shear wave velocity on the lagged coherency of synthetic surface ground motions

E. EL HABER[1,2,*] , C. CORNOU[1], D. JONGMANS[1], F. LOPEZ-CABALLERO[3],D. YOUSSEF ABDELMASSIH[2], T. AL-BITTAR[2]

[1]*Univ. Grenoble Alpes, Univ. Savoie Mont Blanc, CNRS, IRD,IFSTTAR, ISTerre, 38000 Grenoble, France.*

[2]*Scientific Reaserch Center in Engineering, (CSRI), Faculty of Engineering, Geotechnical Engineering, Lebanese University, Lebanon.*

[3]*MSSMat laboratory ,CNRS UMR 8579, CentraleSupélec Paris-Saclay Univ., 3 Rue Joliot-Curie, 91190 Gif-Sur-Yvette, France.*

## Abstract

*The spatial incoherence of ground motion during an earthquake can have a significant effect on the dynamic response of engineering structures such as bridges, dams, nuclear power plants and lifeline facilities. The main objective of this paper is to study the effect of anisotropic heterogeneities in a soil layer overlying homogeneous bedrock on the lagged coherency of surface ground motion. A set of numerical experiments is performed based on 2D spatial variability of shear-wave velocities modeled as a homogeneous stationary random field and discretized by the EOLE method (Expansion Optimal Linear Estimation). Seismic ground motions were simulated using FLAC$^{2D}$ software in the 1-25 Hz band for a plane wave excitation with SV polarization. The soil is characterized by horizontal and vertical autocorrelation distances ranging between 5 and 20 m and 1 and 2 m, respectively, and a coefficient of variation of the shear-wave velocity varying between 5% and 40%. The synthetic seismograms calculated for 9 parameter sets (100 realizations each) clearly show seismic waves scattering and surface waves diffracted locally by the ground heterogeneities, generating large spatial variations in coherence mainly controlled by the coefficient of variation of shear-wave velocity. Consistently with existing models and experimental data, the numerical coherency curves decrease with frequency and receiver distance, however at a rate which is lower than that observed in the experimental data. This difference is probably due to intrinsic attenuation that is not accounted for in the simulations and/or to* our 2D simulations that do not reproduce the complete wavefield. *The numerical average coherency curves for each parameter set*

* elias.el-haber@univ-grenoble-alpes.fr; https://orcid.org/0000-0002-0864-7314 ; Tel: +33 6 29 83 77 28

*exhibit maxima within narrow frequency bands* caused by the vertically trapped body waves and surface wave propagation properties within the average ground model. *This interpretation is supported by experimental data recorded in the Koutavos-Argostoli valley (Greece).*

*Key words: coherency, spatial variability, seismic response, random field, autocorrelation.*

## 1 Introduction

Large earthquakes have often showed spatial variations in damages at the scale from tens to hundreds of meters (e.g. Northridge in 1994 [1] and Christchurch in 2011 [2]). Such spatial distribution can be related to spatial variations of earthquake ground motion (SVEGM; [3]). SVEGM may have remarkable impact on extended and large structures such as bridges and lifelines (see [4] for a summary) and should be considered in the study of their responses and design -[5, 6, 7, 8 and 9]. With regard to seismic design of bridges, SVEGM has been recently incorporated in codes, e.g. EUROCODE8 and Caltrans design procedure [10], that highlighted the importance of assessing it at various spatial scales. SVEGM can be caused by the source mechanism and radiation (magnitude, slip distribution, directivity effects, …), path effects (regional heterogeneities, …) and site effects including both topographical and lithological effects [among others; 11, 12; 13; 14, 15, 16, 17, 18). In addition to these various causes of SVGEM, shallow layers may exhibit spatial heterogeneities resulting from the natural processes of erosion and sedimentation or from human activities (constructions, mining deposits, fills …) [19, 20, 21, 22, 23], which can lead to significant variations in the soil seismic response even at small distances [24]. To account for these local variations, probabilistic modeling approaches using random fields [25] have been widely applied in geotechnical studies [among others, 26, 27, 28]. In earthquake engineering, several studies carried out over the past 20 years have emphasized the effect of the variability of seismic soil properties on SVEGM mainly considering 1D stochastic seismic wave propagation [among other, 29, 30, 31, 32], few studies focusing on 2D stochastic wave propagation [among others; 33, 34, 35, 36, 37, 33].

While the full SVEGM estimation implies determining the phase and amplitude variability [38], the phase variability evaluation has deserved more attention from the scientific community. Indeed, many authors [e.g, 39, 40, 41, 4, 42] have used the complex function called coherency to characterize the phase variability of surface ground motion. Coherency models provide a quantitative measure of the similarity between recordings of the same earthquake at different locations and frequencies [44] and can be used to incorporate SVEGM in the

seismic design of structures [4, 42]. Empirical coherency models have been proposed based on the analysis of ground motions recorded by dense arrays [among others, 44, 45, 40, 46, 47]. Alternatively, other studies have focused on analytical calculations and/or ground motion modeling in isotropic heterogeneous media. They have resulted in semi-empirical coherency models that take into account characteristics of the soil spatial variability in terms of coefficient of variation of shear modulus and related fluctuation scale [48, 49, 50]. However, modeling the soil as an isotropic medium can be unrealistic since the vertical variability of soil is generally greater than the horizontal variability due to natural geological processes that result in a greater distance of horizontal than vertical fluctuation [51, 52, 53]].

The main objective of this paper is to study the effect of the ground spatial variability on the lagged coherency, by performing 2D numerical modeling using statistical parameters found in the literature. We based our study on the geometry and parameters determined for the alluvial plain of Nahr Beirut (Lebanon) [54] and considered a simple 2D model consisting of a soil layer with anisotropic spatial variability overlying a homogeneous elastic bedrock. This model was already used in the paper of El Haber et al. [37] for studying the effect of heterogeneous soil properties on surface ground motion spatial variability. In addition to studying the effect of the spatial variability of soil properties (*V*s) on the spatial coherency properties (average and standard deviation), the numerical results also help to better understand some abrupt variation of coherency within narrow frequency band observed in Koutavos-Argostoli experimental data [55].

## 2 Spatially variable $V_s$ profile generation and wave propagation simulation

In probabilistic approaches, the random field theory is widely used to model the spatial variability of geotechnical and geophysical soil properties [56]. In this paper, the shear-wave velocity (*Vs (x,z)*) is modeled as a random field defined by a probability density function ($pdf$) described by a mean ($\mu_{Vs}$), a coefficient of variation (*COV*) and an autocorrelation function $\rho(\theta x, \theta z)$, $\theta x$ and $\theta z$ being the autocorrelation distances in the horizontal and vertical directions of the 2D medium, respectively. The autocorrelation distance is the distance over which the estimated values of *V*s are not correlated any more. *COV* is defined as the ratio of the standard deviation of *V*s over $\mu_{Vs}$.

The numerical models and ground motion simulation scheme used in this study are identical to those described in the paper of El Haber et al. [37], who numerically studied the effect of 2D soil spatial variability on the spatial variability of earthquake ground motion. The reader may refer to Section 2 of this paper for details on how to

84 introduce ground structure spatial variability into wave propagation simulation. Here, we just recall the main
85 characteristics of the model and the ground motion modeling methods.

86 The soil properties for the parametric study is shown in Table 1. It consists of a 15.5 m thick soil layer with an
87 average $\mu_{Vs}$ =220 m/s, overlying a homogeneous bedrock with *Vs*=1000 m/s. $V_s$ (x,z) in the soil layer is modeled
88 as a 2D random field and the statistical parameters are chosen in a range covering the values found in the
89 literature (5% < *COV* < 40%; 5 < $\theta x$ < 20 m; 1 < $\theta z$ <2 m). The 9 probabilistic models with the different
90 parameter sets are given in Table 1.

91 To discretize the random field *V*s described by a lognormal probability density function (*pdf)* and determine *V*s
92 at the center of each mesh (i.e. midpoint method) [57], we use the Expansion Optimal Linear Estimation (*EOLE*)
93 [58] and the ordinary kriging method [59].

94 For each *V*s realization, the seismic ground motions are calculated using the finite difference code (FLAC$^{2D}$)
95 [60] at 166 receivers located on the surface with a spacing of 1 m by applying a seismic shear stress excitation
96 (vertical incident plane wave of type *SV*) at the base of the 2D model after initializing the stresses. Only the
97 horizontal displacements are fixed along the lateral boundaries of the model, while the horizontal and vertical
98 movements are fixed at its base. Free field boundaries are applied to the side edges of the model. A quiet
99 boundary (absorbing effect defined in FLAC$^{2D}$ [60]), is applied to the model base in order to model a flexible
100 base that absorbs the energy emitted by the waves reflected on the surface and arriving to the model base. The
101 source time function is a pseudo-Dirac having a flat Fourier amplitude spectrum equals to 1 between 1 and 25
102 Hz. No damping is considered in the analysis in order to focus on the effects of elastic properties variability,
103 only.

104 In probabilistic modeling approaches, a large number of discretized *Vs* realizations must be simulated to ensure
105 the statistical convergence of the average and standard deviation estimators of any surface ground motion
106 parameter. This convergence is considered to be reached when the fractions of the relative variation of the
107 average and standard deviation between realization *i* and realization *i+1* are smaller than 5% (for more details
108 refer to El Haber et al. [37]). In this study, for each parameter set, 100 *V*s realizations are sufficient to ensure the
109 statistical convergence of the lagged coherency. The fundamental resonance frequency of the soil layer
110 characterized by a mean $V_s$= 220 m/s and a thickness of 15.5 m is $f_{0D} = 3.54\ Hz$; this case will be referred to as
111 the deterministic model in the following.

Table 1 : Properties of the two layers (soil and bedrock) for the probabilistic modeling. The bedrock properties are fixed, as well as the density $\rho$ and the P-wave velocity $Vp$ in the soil layer. $Vs$ in the soil is considered as a random field and characterized by four statistical parameters ($\mu_{Vs}$, $COV$, $\theta x$ and $\theta z$). Nine parameter sets were defined, combining variations in $COV$, $\theta x$ and $\theta z$ (see text for details) (Modified from El Haber et al. [37]).

| ***Layers*** | ***Properties*** | | | | | | ***Parameter set #*** |
|---|---|---|---|---|---|---|---|
| | $\rho$(Kg/m3) | $Vp$(m/s) | $\mu_{Vs}$ (m/s) | $COV$ (%) | $\theta x$ (m) | $\theta z$ (m) | |
| *Soil* | 1600 | 1500 | 220 | 5 | 5 | 2 | 1 |
| | | | | | 10 | 2 | 2 |
| | | | | 20 | 5 | 2 | 3 |
| | | | | | 10 | 1 | 4 |
| | | | | | | 2 | 5 |
| | | | | | 20 | 2 | 6 |
| | | | | 40 | 5 | 2 | 7 |
| | | | | | 10 | 1 | 8 |
| | | | | | | 2 | 9 |
| *Bedrock* | 2500 | 3000 | 1000 | --- | --- | --- | --- |

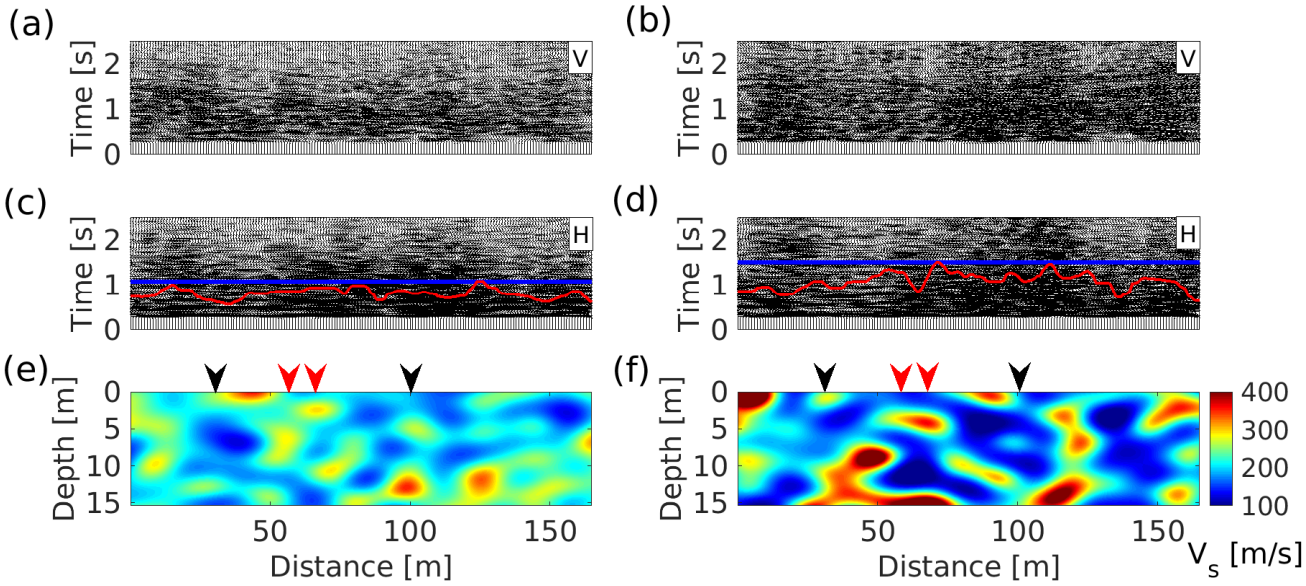


Figure 1: Seismic responses for the two Vs realizations of parameter sets #5 (left column) and # 9 (right column). a) and b) vertical velocities ($V$) computed for the $V$s random field realization shown in e) and f), respectively. c) and d) horizontal velocities ($H$) ; e) and f) $V$s realizations for the parameter sets #5 ($COV$=20% $\theta x$ =10m and $\theta z$ =2m) and #9 ($COV$ =40% $\theta x$ =10m and $\theta z$ =2m), respectively (see Table 1). The red curves correspond to the time ($t_{75\%}$) when 75 % of the total energy (eq. 2) is reached for each seismogram, while the blue lines show the maximum $t_{75\%}$ value calculated for all seismograms of the given realization. The black and red arrows show the receivers located at 30 m and 100 m, and at 55 m and 65 m, respectively.

The synthetic ground motions calculated for one $V$s realization for the two parameter sets #5 ($COV$ =20% $\theta x$ =10m and $\theta z$ =2m) and #9 ($COV$ =40% $\theta x$ =10m and $\theta z$ =2m) (Table 1) are shown in Figure 1. For each parameter set, the $V$s distribution in the sediment layer and the corresponding horizontal and vertical seismograms computed on the surface are presented. The two $V$s distribution shown in Figure 1(e) and (f) highlight the effect of the $COV$ on the generated $V$s profiles, with larger velocity contrasts for parameter set #9 ($COV$=40%) than for parameter set #5 ($COV$=20%). The seismograms (Figure 1a to d) are highly affected by the spatial variation of $V_s$, showing larger amplitude and longer duration at receivers located above low velocity zones, especially for $COV$ =40%.

## 3 Lagged coherency estimation

### 3.1 Definition

The coherency is a normalized complex function given by the ratio between the smoothed-cross spectral density ($S_{jk}$) and the smoothed-power spectral density ($S_{jj}$ and $S_{kk}$) of two signals recorded at location $j$ and $k$ [44]:

$$\bar{\gamma}_{jk}(d_{jk}, f) = \frac{\bar{S}_{jk}(f)}{\sqrt{\bar{S}_{jj}(f).\bar{S}_{kk}(f)}} \quad (1)$$

where $d_{jk}$ is the distance between location $j$ and $k$, and $f$ is the frequency.

From the complex coherency function presented in Eq. 1, several real coherency functions can be used: lagged coherency, unlagged coherency, and plane-wave coherency [61]. The lagged coherency ($\gamma_{jk}^{L}$) is the amplitude of the complex coherency function ($\bar{\gamma}_{jk}$) (Eq. 1). At low frequency and small inter-receiver distance, ground motions are close and the corresponding lagged coherency tends to 1. In contrast, for large distance and high frequency, $\gamma_{jk}^{L}$ decreases down to 0.

After pre-aligning the signals in time by using the time lag leading to the maximum cross-correlation, the lagged coherency is the most commonly used indicator to measure the seismic motion similarity [44, 45, 46, 47]. Indeed, its use is assumed to eliminate the deterministic variation in surface ground motion caused by the wave propagation, keeping only the stochastic variation [61]We use the lagged coherency in this paper to evaluate the impact of the spatial variability of soil properties on the phase variability of synthetic ground motions.

### 3.2 Coherency function smoothing

In the lagged coherency estimation, a frequency smoothing process of the seismic time histories spectra is mandatory [44]. Indeed, when no smoothing window is used, the phase difference terms disappear from the covariance spectra and the lagged coherency estimate is unity for any frequency and any receiver distance [62]. This process also controls the statistical properties (i.e variance and bias) and the resolution of the coherency estimates. The increase of the smoothing bandwidth leads to a decrease in coherency estimation uncertainty while decreasing however the resolution. Thus, the smoothing type and parameter have to be well chosen to find

a balance between uncertainty and resolution of the estimated coherency. According to Harichandran [41], the most common smoothing type windows (e.g. hamming, cosine, triangular, …) yield similar results as long as the equivalent spectral bandwidths are the same. Abrahamson et al. [61] proposes an 11-point Hamming window ($2M + 1$; where $M$ is the Hamming parameter) for the spectral smoothing of the time windows containing less than 2000 samples when the coherency estimates are to be used in structural analysis with damping coefficient of 5%. In this study, the cross- and auto-spectral densities in equation Eq. 1 are smoothed using an 11-point ($M = 5$) Hamming window, corresponding to a spectral bandwidth of 1.95 Hz. The synthetic ground motions calculated at the surface are resampled to a rate of 50 Hz with 256 samples.

### 3.3 Time window selection

The shear (S-) wave part of seismograms is commonly used to estimate the coherency function as it is considered as the the most damaging seismic phase for civil engineering structures [43, 45, 63]. However, the identification of S-waves in seismograms is sometimes difficult because they are often accompanied by other waves due the scattering and diffraction in the heterogeneous medium [63]. Although the selection of the S-wave window can be made visually, Abrahamson [43] proposed an automatic process based on the duration of the normalized Arias Intensity *AI* (Eq. 2):

$$AI_{i,n}(\tau) = \frac{\int_0^{\tau} v_{i,n}^2 dt}{\int_0^{end} v_{i,n}^2 dt} \quad (2)$$

where $v_{i,n}$ corresponds to the horizontal velocity component calculated at the receiver $i$ of the realization $n$ and $\tau$ indicates time.

The criterion used by Abrahamson [43] is that the S-wave time window corresponds to *AI* between 0.1 and 0.75, the lower limit being chosen to remove the P-wave firstly arriving at the surface. As we generate a plane wave of SV type, the S-wave time window in this study is defined for *AI* between 0 and 0.75 (Eq. 2).

As shown in Figure 1c and d, the horizontal velocities are highly affected by the shallow *V*s structure, leading to significant variations in duration and amplitude. For the horizontal component, the time corresponding to *AI* equal to 0.75 ($t_{75\%}$) are shown in red for the two *V*s realizations in Figure 1c and d. The rise in *COV* (40%) clearly increases $t_{75\%}$ (Figure 1d), particularly for receivers located above superficial low velocity zones. In

literature, the lagged coherency estimation is based on the selection of the same time window for all the recordings of the same event [43, 64]. Accordingly, the time window used to estimate the lagged coherency between seismograms of the same realization was chosen as the maximum $t_{75\%}$ (blue line) of this realization (Figure 1c and 1d). Even though $t_{75\%}$ is calculated using seismograms on the horizontal component, the same time window is used for the lagged coherency estimation of both the horizontal and vertical component.

### 3.4 Average and standard deviation

For statistical analysis on the coherency estimates, normally distributed data are preferable [41]. Hence, the *atanh* of lagged coherency is used to produce an approximately normal distribution with a bias that can be estimated and removed [65].

Following Harichandran [41] and Abrahamson et al. [61], the statistical analyses of the lagged coherency are performed on *atanh(γ)* instead of $\gamma$ and the average and standard deviation of the lagged coherency are calculated as follow:

$$\gamma = \gamma(d,f)|_{mean} = \tanh\left(E\left(Atanh\left(\gamma_{jk}^{L}\right)\right)\right) \quad (3)$$

$$\sigma(\gamma) = \gamma(d,f)|_{std} = \tanh\left(\sqrt{S\left(Atanh\left(\gamma_{jk}^{L}\right)\right)}\right) \quad (4)$$

where $E$ is the mathematical expectation, $S$ is the variance defined by $S(X) = E(X^2 - E(X)^2)$ for a variable $X$ and *std* denotes the standard deviation.

At a frequency of 3.54 Hz (the fundamental frequency of the deterministic model) and for the parameter set #9 ($COV$ =40% $\theta x$ =10m and $\theta z$ =2m; Table 1) that exhibits the largest $V$s range, Figure 2a and b show the distribution of the lagged coherency $\gamma_{jk}^{L}$ from 100 $V$s realizations and two inter-receiver distance, $d$ = 10 m and $d$ = *70 m*, respectively. It is clear that $\gamma_{jk}^{L}$ is not normally distributed regardless the inter-receiver distance, while the distribution of $atanh(\gamma_{jk}^{L})$ shown in Figure 2c and d can be fitted by a normal distribution.

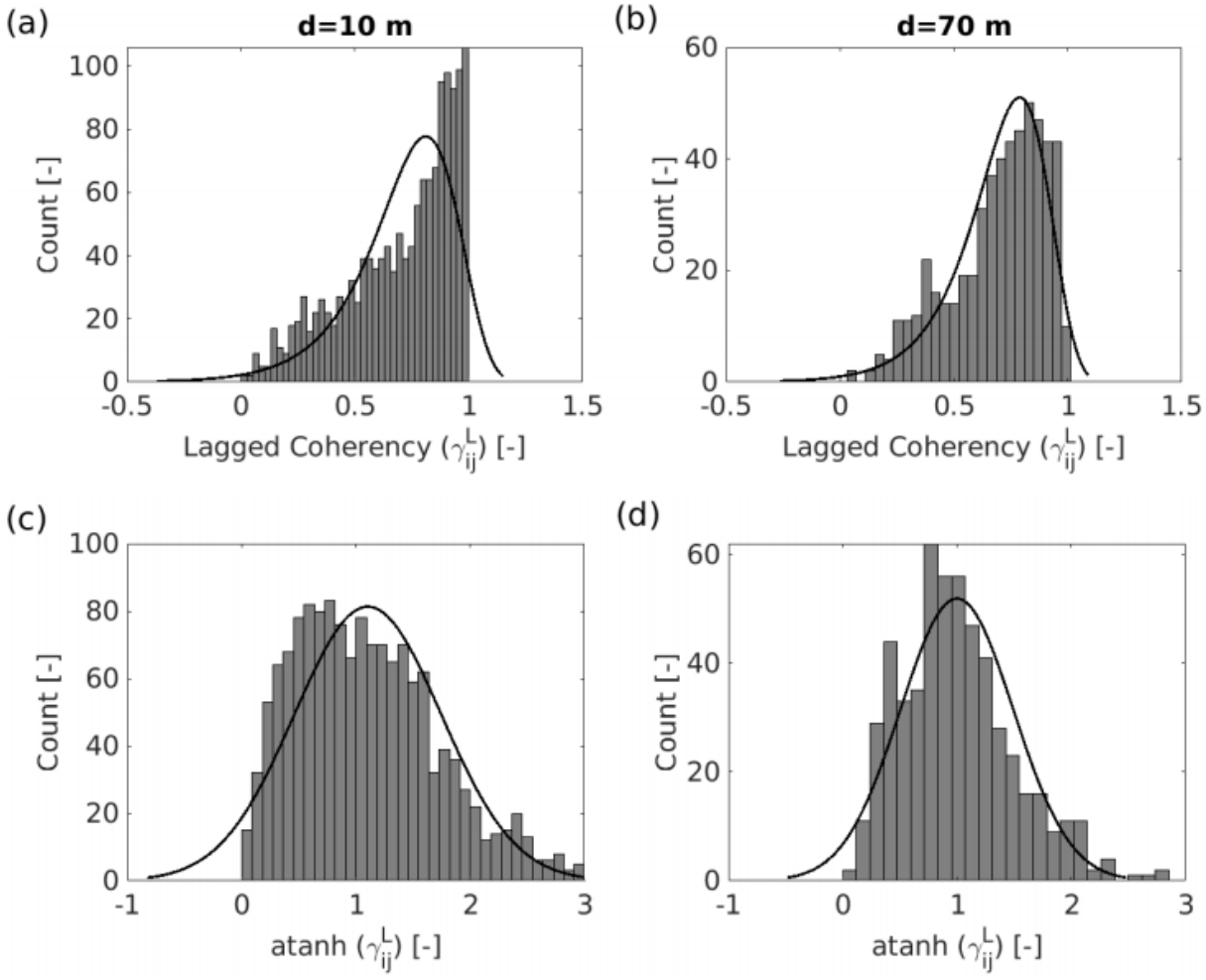


*Figure 2: Statistical distribution of the lagged coherencies: a) and b) Histograms of the lagged coherencies ($\gamma_{jk}^{L}$) calculated between receivers separated respectively by d = 10 m (left column) and d = 70 m (right column) for all realizations of the parameter set #9 (COV =40% θx =10m and θz =2m) and for a frequency of 3.54 Hz. c) and d) Histograms of atanh transformation of γ in a) and b) respectively. a) and b) are fitted by an Extreme Value distribution and c) and d) are fitted by a Normal distribution (continuous lines).*

### 3.5 Stationarity of lagged coherency

An important aspect in the use of random field modeling approach is to ensure the stationarity of the output average estimates. We thus compare the lagged coherency variability obtained when using 100 stochastic *V*s profiles for one receiver pair and when using all receivers pair for a given realization. Figure 3a and b show the coherencies calculated for all pairs of receivers separated by a distance *d* =70 m for the two realizations

213 presented in Figure 1e and f, respectively, while Figure 3c and d shows the coherencies calculated between
214 receivers located at 31 m and 101 m (black receivers in Figure 1e and f) for the 100 realizations of the two
215 parameter sets #5 and #9 (Table 1), respectively. The bold solid and dashed curves represent the average
216 coherency +/- one standard deviation using Eq. 2 and Eq. 3. The four figures show that the coherency curves
217 vary with the location of the receivers on the surface and the *V*s realization. However, the comparison of the
218 average coherency in Figure 3e and f indicates almost similar coherency values. This comparison clearly outlines
219 the lagged coherency stationarity by using the *EOLE* random field modeling approach and indicates that the
220 estimated average coherency curves are robust. In the following sections, the average and standard deviation of
221 the coherency will be computed for all *V*s realizations, using all receivers except those located within 30 m of the
222 model boundaries.

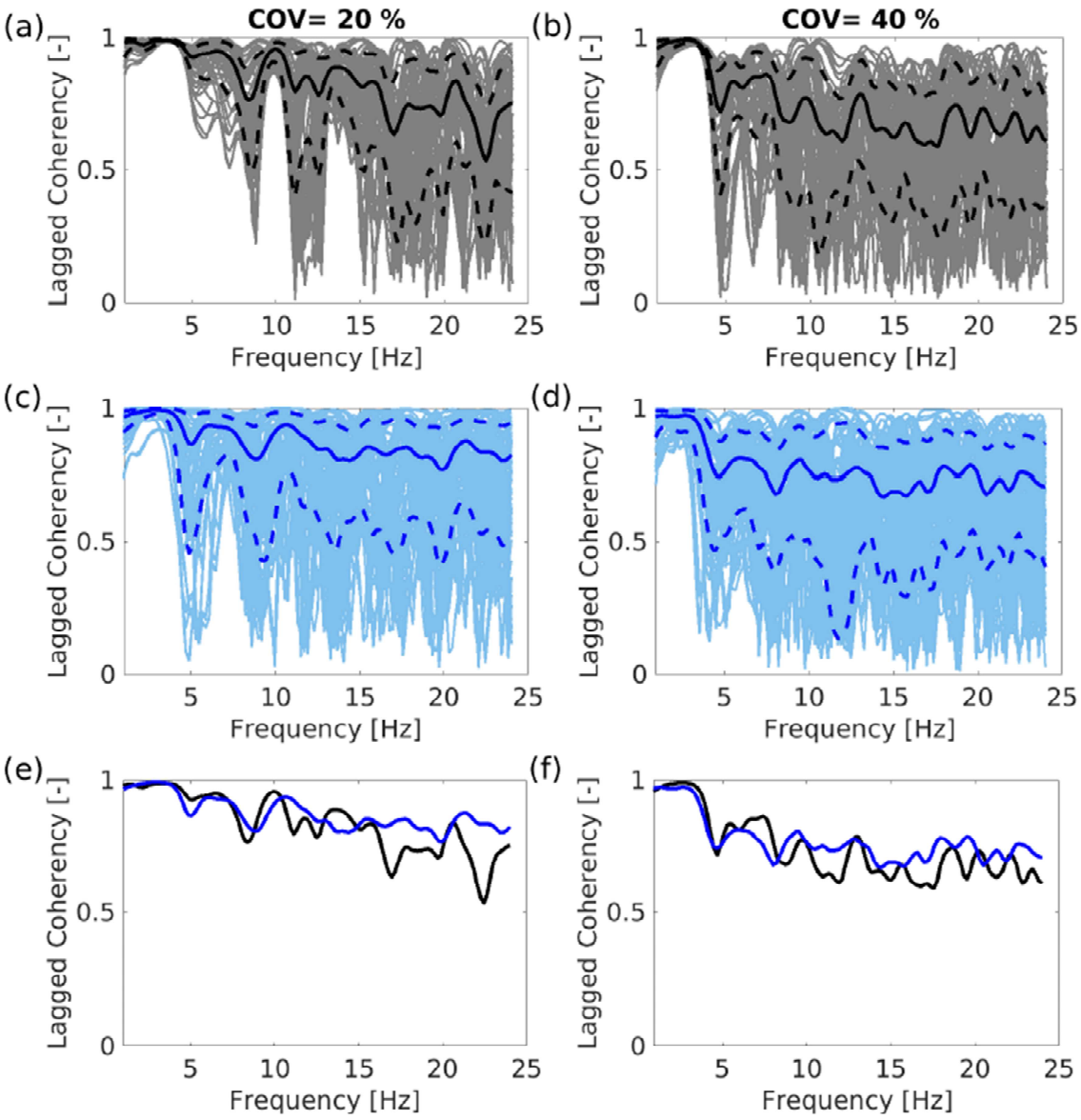


223

224 *Figure 3: Lagged coherency curves (horizontal velocity) calculated for parameter sets #5 (left*
225 *column) and #9 (right column), (see Table 1). a) and b) curves for all the receiver pairs*
226 *separated by a distance d = 70 m (in grey ) for the two Vs realizations shown in Figure 1e*
227 *and Figure 1f, respectively. c) and d) curves computed between the receivers at 30 and 100m*
228 *(in light blue) for the 100 Vs realizations. The bold solid and dashed curves represent the*
229 *average and the average +/- one standard deviation, respectively. e) and f) superposition of*
230 *the average curves shown in a) and c), and in b) and d), respectively.*

231

## 4 Effect of the ground heterogeneities on the average lagged coherency

Our study is focused on the lagged coherency computed for the horizontal component of the ground motion, which is the most studied in the literature (Imtiaz et al.,2018a) because of its impact on the behavior of structures and the importance given to it in seismic design codes. Results along the vertical component will be briefly commented and given in appendix A2.

The average lagged coherency ($\gamma$) of the horizontal component is calculated for all the parameter sets given in Table 1 and shown in Figure 4 for 4 receivers distances (from $d$ = 5 to 70 m). The main trend is that $\gamma$ decreases with the frequency and $d$, with a much more pronounced decrease effect when $COV$ increases. The effect of the horizontal and vertical autocorrelation distances ($\theta x$ and $\theta z$) is weak and can only be observed for large $COV$ (40%) (Figure 4) and for $d$=5 m and $COV$ = 20% (Figure 4a), with the trend that $\gamma$ decreases with the decrease in $\theta x$. All average coherency curves computed for large $d$ values (Figure 4c and d) exhibit two minima at 4.8 Hz and 8.5 Hz, respectively, which are more pronounced for large COV values.

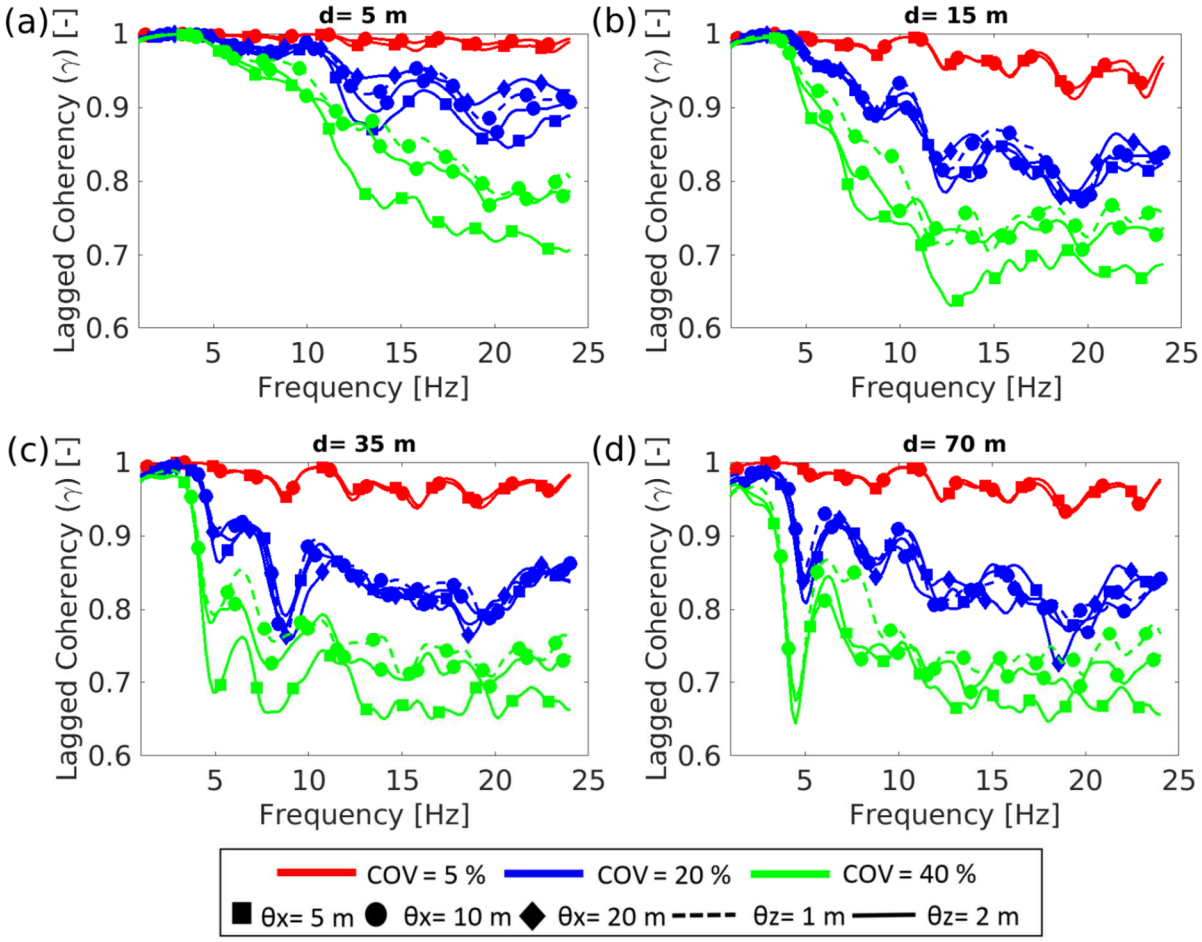


Figure 4: Average lagged coherency ($\gamma$) calculated using the horizontal velocity, for different values of *COV*, $\theta x$ and $\theta z$ for the 100 realizations computed by using the *atanh* transformation (see text for details) for four receivers' distances: a) $d = 5\ m$, b) $d = 15\ m$, c) $d = 35\ m$ and d) $d = 70\ m$.

Figure 5 presents the average coherency curves calculated for all inter-receiver distance and for each of the 9 parameter sets (Table 1). Minima and maxima of the average coherency within the same narrow frequency bands are systematically observed whatever the parameter set considered, particularly for large distance ($d > 25\ m$). This consistency suggests that curve extrema (minima and maxima) are controlled by the average properties of the soil layer. To understand these results, an equivalent 1D model per parameter set is defined to reproduce the measured fundamental resonance frequency picked on the average amplification function *AF(f)* from the 100 realizations. The calculation process is described in Appendix 1. From these equivalent models, the group velocity dispersion curves ($V_G$) of the Rayleigh waves are computed using the method proposed by Dziewonski et al. [66] and improved by Levshin et al. [67]. The average amplification function *AF(f)* and the group velocity dispersion curves of the first higher modes are plotted in Figure 5a to 5j for the 9 parameter sets. The computed

amplification curves exhibit several peaks (around 3.5, 10.5 and 17.5 Hz, i.e. at the resonance frequencies of the soil column) with a decrease in the peak amplitude with frequency and *COV*. As there is no attenuation in the numerical ground motion simulation, this attenuation effect results from the scattering generated by the heterogeneities. The larger the *COV* is the higher the apparent attenuation. Comparing the average coherency and amplification curves, we can see that the amplification peaks approximately coincide with maxima of the coherency curve. At resonance frequencies indeed, the vertical reverberation of S-waves are in-phase, leading to high $\gamma$ values. Between the resonance frequencies, $\gamma$ tends to decrease due to wave scattering, particularly for large *COV* values (Figure 5h to 5j). However, there is a systematic coherency increase (slight to strong, depending on *COV*) between the fundamental resonance frequency and first harmonic. This increase coincides with the Airy phase frequency of the fundamental mode of Rayleigh wave group velocity (minimum in the dispersion curve in Figure 5a to i), which corresponds to a very energetic in-phase motion [68] and lead to high $\gamma$ values. In our case, the Airy phase frequency of the first Rayleigh wave mode is in the same range as the second resonance frequency (10.5 Hz).

A similar study is conducted for the vertical component of the ground motion. The average lagged coherency curves are given in Appendix 2 for all the parameter sets and receivers distances ranging from $d$ = 5 to 70 m. The main results outline that coherency curves exhibit sinusoidal shapes for small COV (5%), however rapidly damped with frequency for large COV (20% and 40%). The autocorrelation distances have small influence on the coherency curves. The first maximum of the coherency curves again coincides with the fundamental frequency of the deterministic model ($f_0 = 3.54\ Hz$). As the input motion is a pure SV wave, this result also outlines that scattered S-waves by soil heterogeneities distribute energy on the vertical component.

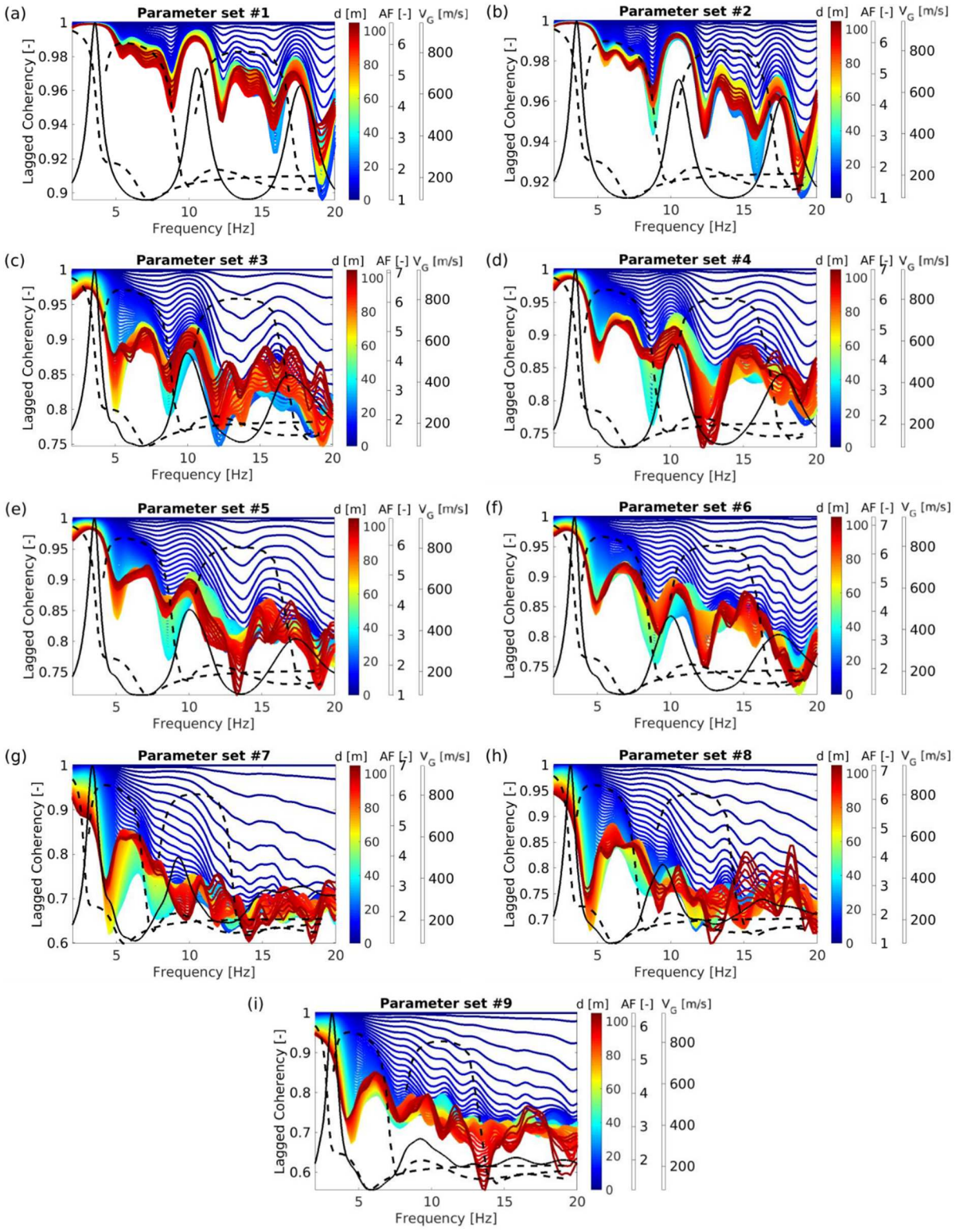


279

280 *Figure 5: Average lagged coherency ($\gamma$) for different receivers' distances in color curves, the*
281 *average amplification function ($AF$) in solid black and the Rayleigh group velocity curves*
282 *($V_G$) for the three first modes in dashed black calculated for the nine parameter sets in table*

*1. The coherency scale is different for each parameter set. The vertical axis of AF and $V_G$ are displayed to the right of the distance (d) colorbar.*

## *5 Comparison with experimental data and existing models*

### 5.1 *Comparison between numerical and experimental data*

A very dense seismological array was deployed on the site of Koutavos-Argostoli (Greece), which is a small valley characterized by a soil thickness of maximum 80 m and a resonance frequency of about 1.5 Hz [69, 70]. Below the array, shear-wave velocity in the sediment gradually increases from 150 m/s to 400 m/s and the seismic bedrock is at 60 m depth [63]. Using a set of 46 earthquakes, with magnitude ranging from 2 to 5 and epicentral distances up to 200 km, Imtiaz et al. [55] calculated average lagged coherencies for distances between receivers ranging from 10 to 90 m. The coherency curves for the horizontal component (Figure 6) exhibit shapes with a strong decrease with frequency and receivers' distances, leading to coherency values lower than 0.5., suggesting that the soil layer is heterogeneous. However, the intrinsic attenuation, which is not considered in the numerical simulations, and our 2D simulations that do not account for the complete wavefield, could also play a role on the coherency curve shape at high frequency and explain the low coherency values obtained in the experimental data.

The other point to emphasize is the progressive apparition of minima and maxima at specific frequencies with the receiver distance increase. Between 2 and 8 Hz, the experimental lagged coherency curves (Figure 6) exhibit three maxima at about 2, 4.8 and 6.5 Hz, for the larger receivers' distances. Other extrema are also observed at higher frequencies, especially for receiver distances of 30-40 m and 80-90 m. In the same figure, the theoretical amplification function and the dispersion curves of the three first modes (group velocity, Rayleigh waves) computed from shear-wave velocity profiles [63, 71] are plotted. In this case, the Airy phase frequencies of the first two Rayleigh wave modes are close to the first resonance harmonic, while the third Rayliegh wave mode frequency is in the same range as the second harmonic. Similarly to the numerical results, the maxima of the lagged coherency in the low frequency range (here 0-8 Hz) approximately coincide with the first three peaks of amplification and the Airy phase of the Rayleigh waves. These theoretical and experimental results obtained for a sediment layer over bedrock suggest that the maxima within narrow frequency range of coherency in the low

frequency range (up to two to three times the fundamental resonance frequency of the site) are mainly influenced by the average 1D soil properties (mean Vs and thickness) that control the Airy phase and resonance occurrence frequencies. At these frequencies, the S and Rayleigh waves are propagating in phase and carry most of the seismic energy, explaining the maxima of the lagged coherency. At higher frequencies, seismic waves are highly diffracted leading to low average coherency values.

These results contradict the few previous analyses suggesting that the minimum in the coherency functions coincide with the fundamental frequency of the site [72, 73]. Based on this interpretation and on the Luco and Wong [48] model, Zerva and Harada [74] proposed a new coherency model depending on the average and standard deviation of the estimated fundamental frequency of the medium and exhibiting a coherency drop at the fundamental frequency. Further studies involving detailed experimental data from other sites will need to be carried out to understand these differences in interpretation.

Imtiaz et al. [63, figure 9 in their paper] also provided experimental average coherency curves for the vertical component, which show a first maximum at the fundamental frequency and a significant downward trend at higher frequencies. This curve shape is consistent with the numerical results for high *COV* values (≈ 40%; appendix 2), again suggesting that the soil cover at Koutavos-Argostoli is spatially highly heterogeneous.

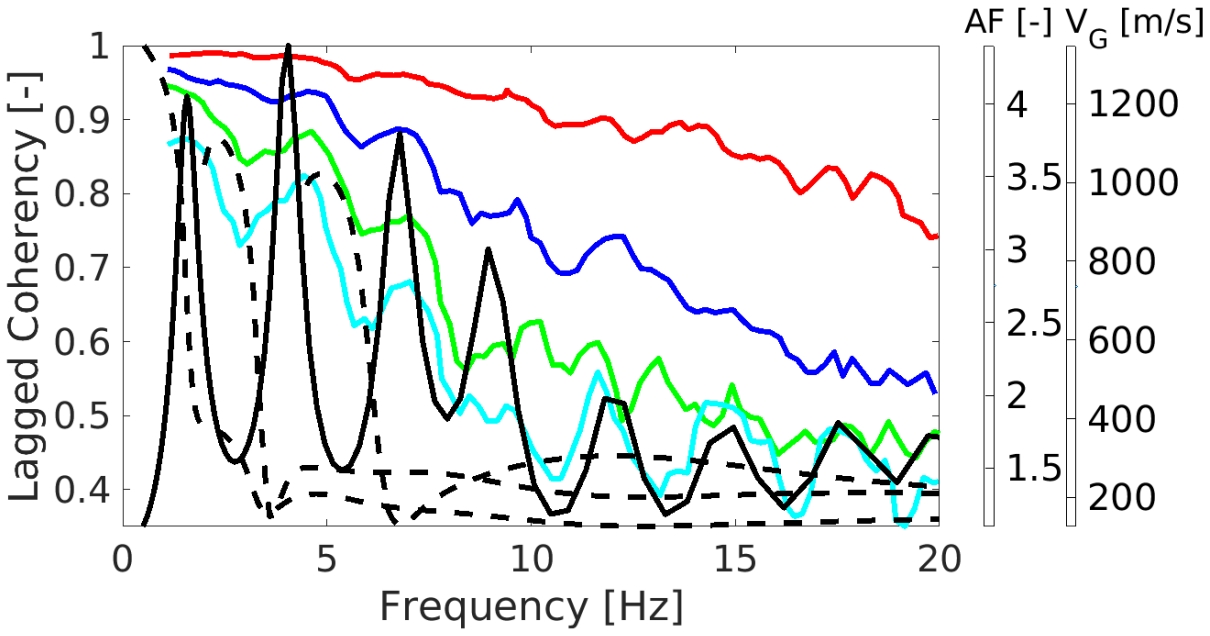


*Figure 6: Experimental average lagged coherency (γ) curves in color, the average amplification function (AF) curve in solid black and the Rayleigh group velocity curves ($V_G$)*

*for the three first modes in dashed black calculated in the valley of Koutavos-Argostoli (Imtiaz et al., 2017). Coherency curves are shown for four distances between receivers: 10-20 m (red curve), 20-30 m (blue curve), 30-40 m (green curve) and 80-90 m (cyan curve). The vertical axis of AF and $V_G$ are displayed to the right of the distance (d) colorbar.*

### *5.2 Comparison with existing models*

The computed coherency curves (horizontal motion) are compared to four parametric coherency models used in the literature for engineering application: the theoretical coherency model of Uscinski [75], the semi-empirical model of Luco and Wong [48], the semi-empirical model of Sato et al. [49] and the empirical model of Abrahamson et al. [60]. These coherency models are usually used

The coherency model of Uscinski [75] is derived from the analysis of shear waves propagating a distance $H$ through a random medium. The lagged coherency for a pair of ground motions as a function of inter-receiver distance ($d$) and angular frequency ($\omega$) is given by:

$$\gamma(d,\omega) = \exp\left(-\omega^2\theta H\frac{COV^2}{V_s^2}\left(1-\exp\left(\frac{d^2}{\theta^2}\right)\right)\right) \quad (6)$$

where $\theta$ is the correlation length of random inhomogeneities along the path, $COV$ is a measure of the relative variation of elastic properties, $\omega$ is the angular frequency, $V$s is an estimate of the elastic wave velocity and $d$ is the receiver distance. In this study, $H$ is the depth of the heterogeneous soil layer.

By simplifying this coherency model, Luco and Wong [48] proposed to express the coherency for receiver distance ($d$) and an angular frequency ($\omega$) as follows:

$$\gamma(d,\omega) = \exp\left(-\omega^2\left(\frac{COV}{V_s}\sqrt{\frac{H}{\theta}}\right)^2 d^2\right) \quad (7)$$

From theoretical considerations on seismic wave propagation in random heterogeneous media [49] gave the functional form of the coherency model as:

$$\gamma(d,\omega) = \exp\left(-\sqrt{\pi}\omega^2\theta H\frac{COV^2}{V_s^2}\left(1-\exp\left(\frac{d^2}{\theta^2}\right)\right)\right) \quad (8)$$

Finally, the majority of the empirical coherency models in the literature are elaborated for receiver distance larger than 100 m. However, Abrahamson et al. [61] coherency model was developed from the horizontal seismograms recorded by a small array (LSST) in Taiwan and allows the estimation of the lagged coherency for receiver distance smaller than 100 m. The lagged coherency is given by:

$$\gamma(d,f) = \tanh\left((2.54-0.012d)\left(\exp\big((-0.115-0.00084d)f\big)+\frac{f^{-0.878}}{3}\right)+0.35\right) \quad (9)$$

where $f$ is the frequency.

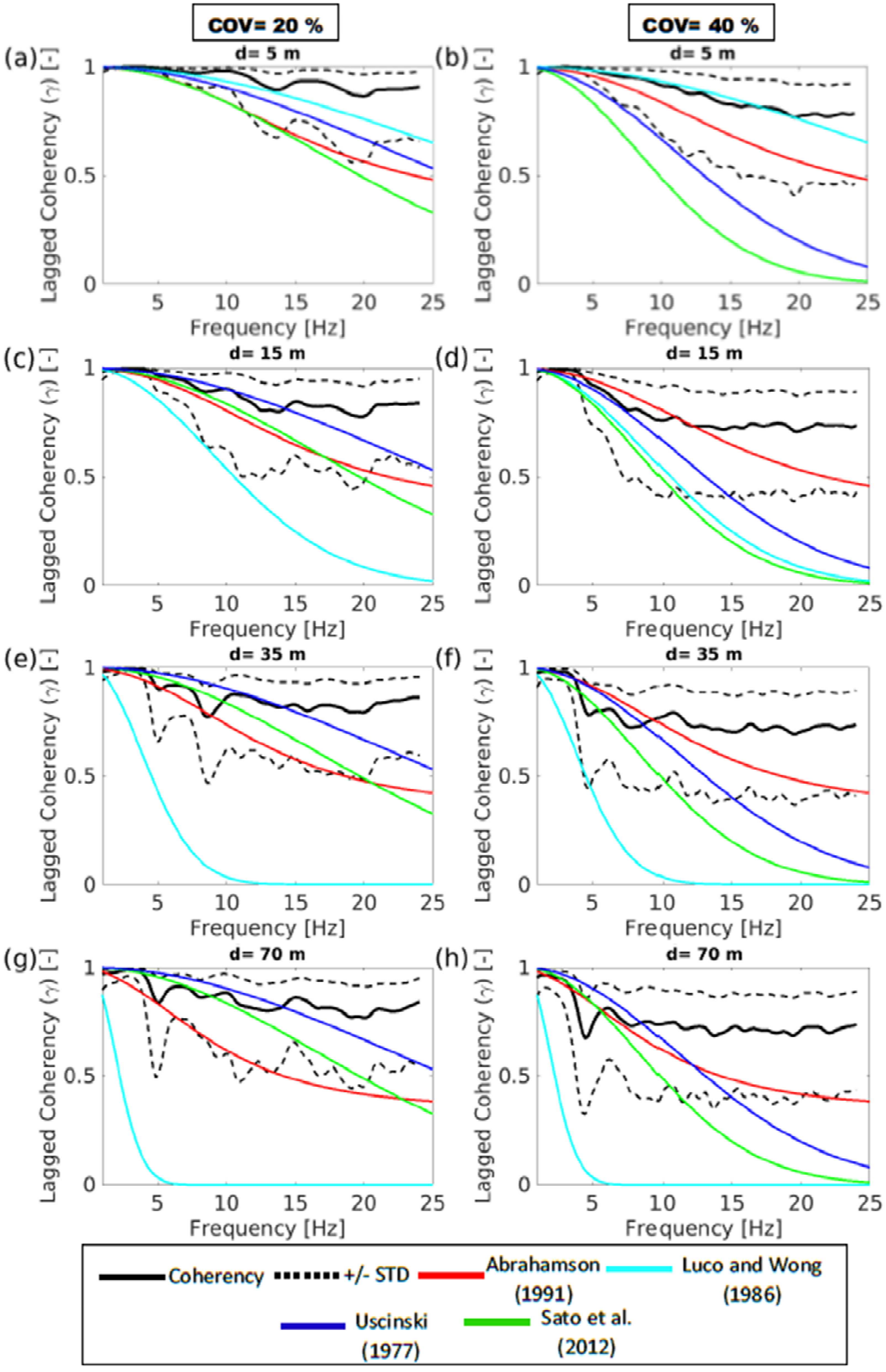


356

357 *Figure 7: The average lagged coherency +/- one standard deviation (in black) for parameter*

358 *set #5 (COV =20% θx =10m and θx =2m) (left column) and parameter set #9 (COV =40% θx*

359 *=10m and θx =2m) (right column) in Table 1 for 4 receiver distances: (a) and (b) for d =5 m,*

*(c) and (d) for d =15 m, (e) and (f) for d =35 m and (g) and (h) for d =70 m compared with the coherency models of Abrahamson et al. [61] in red, Luco and Wong [48] in cyan, Uscinski [75] in blue and Sato et al. [49] in green.*

Figure 7 compares the average lagged coherency ($\gamma$) computed for the two parameter sets #5 and #9 having the same autocorrelation distances ($\theta_x$=10m and $\theta_z$=2m) and different *COV* (20% and 40%, respectively), with the aforementioned four coherency models for the four receivers' distances: $d$ = 5 m, $d$ = 15 m, $d$ = 35 m and $d$ = 70 m. Although the coherency model of Luco and Wong [48] correctly predicts the coherency for small $d$ and large *COV* (Figure 7b), it largely underestimates the coherency for large d (Figure 7g and h). Furthermore, even if the model of Sato et al. [49] provides lower coherencies than the one of Uscinski [75], these 2 coherency models are very similar to each other. They are not appropriate for very small distances ($d$ = 5 m) (see Figure 7a and b), but they better estimate the coherency for the parameter set having a COV of 20% (left column) than the one with a COV of 40% (right column) especially for low frequencies. Finally, the coherency model of Abrahamson et al. [61] gives relatively a good estimate of the coherency at low frequencies (below 7 Hz), but underestimate it at high frequencies. It seemingly fits better the parameter set #9 (*COV* =40%) than parameter set #5 (*COV* =20%), being within the computed average coherency +/- one standard deviation range. However, none of the four coherency models predict the coherency extrema in narrow frequency ranges observed for the synthetic simulations and at the Koutavos-Argostoli array. It outlines the need of further development of coherency models able to reproduce both the general decay of coherency with frequency of distance and extrema in narrow frequency bands.

## 6 Effects of the ground heterogeneities on the standard deviation of the coherency

As outlined in previous sections, decrease of $\gamma$ with frequency and inter-receiver distance is clearly controlled by *COV*, while influence of the vertical and horizontal autocorrelation distances are not significant except for large *COV* and small inter-receiver distance (Figure 4). Interestingly, the influence of *COV* on $\gamma$ is not observed on the standard deviation ($\sigma(\gamma)$, Eq. 4) whatever the parameter sets. Figure 8a to d presents $\sigma(\gamma)$ for four inter-receiver distances ranging from 5 to 70 m : for a given *COV*, $\sigma(\gamma)$ curves are rather similar for the different receiver distances, being only slightly influenced by the auto-correlation distances $\theta_x$ and $\theta_z$. At low frequency (around 5 Hz), $\sigma(\gamma)$ exhibit similar values for all *COV* and autocorrelation distances, while $\sigma(\gamma)$ tends to decrease with *COV*

388 at high frequencies. This observation is surprising in view of Figure 3, which shows that individual coherency
389 curves are more variable for large *COV* values. The standard deviation of $\sigma(\gamma)$ should intuitively increase with
390 *COV*, which is not the case because of the *atanh* transformation of lagged coherency (Eq. 4)

391 In order to better account for larger variability of individual lagged coherency curves for larger COV in standard
392 deviation of average lagged coherency, we propose to use another distribution function to fit the lagged
393 coherency curves. Given that the lagged coherencies exhibit a maximum equal to unity for all the receiver-pairs
394 and for different frequencies (Figure 3), the Extreme Value (*EV*) distribution (Type I) function is a good
395 candidate for random variables having a minimum/maximum extreme [76]. The *EV* function is defined by:

396

$$f(x) = \frac{1}{\sigma'} e^{-e^{-\frac{x-\mu'}{\sigma'}} - \frac{x-\mu'}{\sigma'}} \qquad (5)$$

397

398 where $\mu$' and $\sigma$' are the two parameters that can be associated to $\mu$ and $\sigma$ of the normal distribution function,
399 respectively.

400 Figure 2(a) and (b) illustrates the fit of lagged coherency with the *EV* distribution

401

402

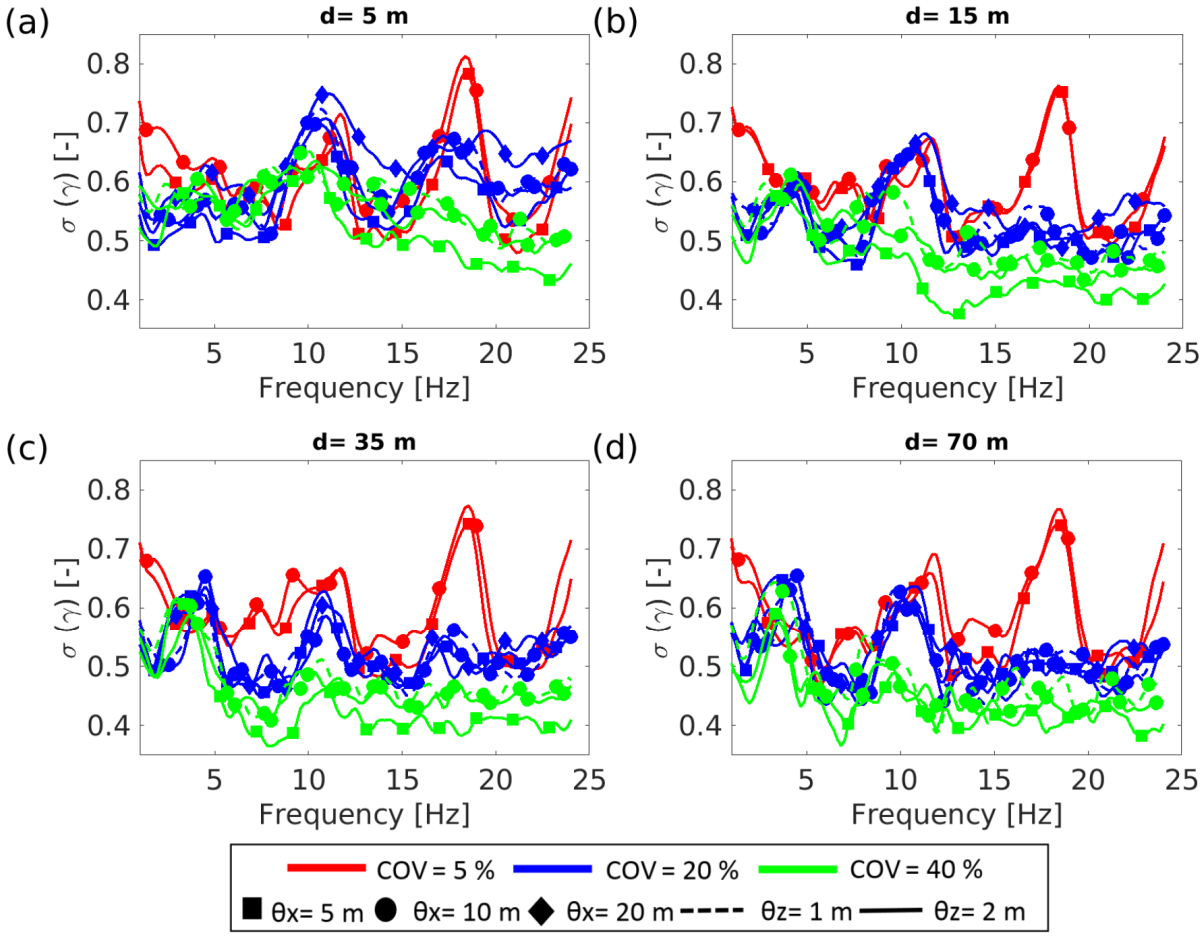


403

404 *Figure 8: The standard deviation of the lagged coherency (horizontal component) calculated*
405 *using the atanh transformation for different values of COV, θx and θz, and for four receivers'*
406 *distances: a) d = 5 m, b) d = 15 m, c) d = 35 m and d) d = 70 m.*

407 Figure 9 shows the average and the standard deviation of the lagged coherency calculated by using the *EV*
408 distribution function for 4 receiver distances ranging from 5 to 70 m. The average coherency curves (left
409 column) are similar to those shown in Figure 4 obtained using the *atanh* transformation with slightly lower
410 values and with minima at the same frequencies.

411 Standard deviations calculated using the *EV* distribution (Figure 9, right column) clearly outlines the increase of
412 $\sigma(\gamma)$ with *COV* for all frequencies and receiver distances and, for large inter-receiver distances, at the frequencies
413 corresponding to the coherency minima.

414 These results outline the interest of using the *EV* distribution to picture the effects of ground heterogeneities both
415 on the average lagged coherency and the related standard deviation. It also opens perspective to infer *COV* at a
416 site based on the joint properties of the average and variability of the lagged coherency.

417

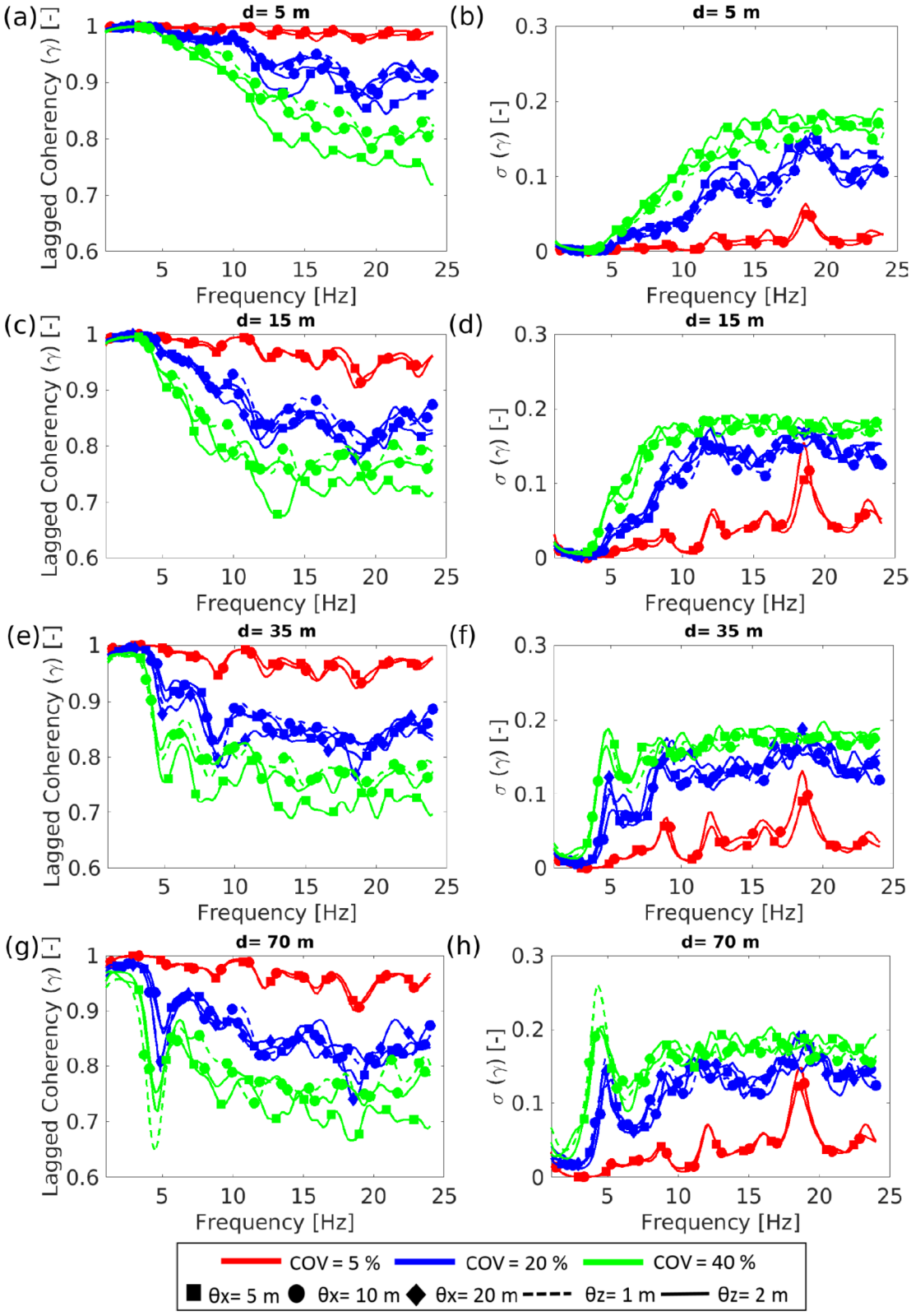


418

419 *Figure 9: The average (γ) (left column) and the standard deviation (σ(γ)) (right column) of*

420 *the lagged coherency calculated for the horizontal component and using the Extreme Value*

421 *distribution. Computations are made for different values of COV, θx and θz for receiver*

*distances of d = 5 m (a) and (b), d = 15 m (c) and (d), d = 35 m (e) and (f) and d = 70 m (g) and h).*

## 7 Conclusions

A numerical probabilistic study for a simple velocity structure (an elastic heterogeneous sedimentary layer over a homogeneous half-space) is performed in order to investigate the effect of the *Vs* spatial variability on the lagged coherency of ground motion. Nine parameter sets were built by varying the following three $V_s$ statistical parameters: the coefficient of variation (*COV*) and the horizontal and the vertical autocorrelation distances ($\theta x$ and $\theta z$). The analysis of the simulated synthetic seismogram at surface shows that the average lagged coherency values (horizontal component) exhibit the same shape for all parameter sets with a decrease as frequency or -receiver distance increase. The main parameter controlling the decrease of the average lagged coherency is the coefficient of variation (*COV*,) autocorrelation distances ($\theta x$ and $\theta z$) having only negligible effects except for small receivers' distances in the high frequency range. For engineering application, geotechnical and geophysical tests (e.g.: *Vp* and *Vs* tomography tests) should be carried out to measure the most important statistical parameters of the soil (the mean and the coefficient of variation) in order to reduce the uncertainty on the prediction of the surface ground motion variability.

Synthetic coherency curves exhibit extrema (maxima or minima) within narrow frequency bands in-between the resonance frequency of the site up to the second to third overtones, which are not predicted by coherency models. Such extrema (maxima) are controlled by the average properties of the site, namely resonance frequencies and Rayleigh wave Airy phase frequencies. Indeed, at those frequencies, seismic motions at surface are in-phase and therefore lead to large coherencies. This interpretation is very consistent with the experimental coherencies observed in the valley of Koutavos-Argostoli [55]. Finally, our interpretation is that coherency decreases with frequency or distance as result of seismic wave scattering at ground heterogeneities, modulated at specific frequencies by high coherency values due to the body and surface wave propagation within the average ground model.

Comparison between synthetic average coherency curves (horizontal component) and existing coherency models used for engineering applications outlines that existing models underestimate the coherency for all parameter sets. However, this probabilistic numerical study is limited to an elastic soil behavior and intrinsic attenuation could explain at least partly the observed discrepancy. Anyhow, none of the tested existing models are enable to

capture the variation of coherencies within narrow frequency bands. Thus, new coherency models shall be developed in the future to better reproduce these sudden variations that may have significant importance for soil-structure interaction applications.

Moreover, we showed that the $atanh$ transformation of individual coherencies recommended by Abrahamson et al. [61] to compute the standard deviation is not relevant if one wants to relate statistical parameters of the underground velocity structure and lagged coherency in terms of average and standard deviation. Instead, we propose a new measure of average and standard deviation based on the Extreme Value (*EV*) distribution (Type I). We show that this distribution provides average coherency close to the one inferred from $atanh$ transformation and standard deviation clearly sensitive to the *COV*.

Finally, the simple case of a sedimentary layer over a bedrock does not represent the real site conditions, even though it provided interesting findings regarding the relationships between underground heterogeneities and the ground motion variability observed on surface. To confirm our results, further numerical simulations, including 3D ground models, should be carried out for a set of typical ground structure with various *V*s profiles, various seismic impedances and sediment thickness, considering also attenuation and non-linear soil behavior. Dedicated measurements at well-known instrumented sites will also help assessing the relationships between ground spatial heterogeneities and observed lagged coherencies in terms of average value and standard deviation.

# 8 Appendices

## Appendix 1: 1D equivalent models

We define 1D equivalent deterministic models for each parameter set, based on the computation of the amplification function *AF(f)*. For each parameter set (Table 1), *AF(f)* is the average over the 100 realizations of the ratio between the Fourier amplitude spectra of the signals recorded at the central receiver and the outcropping bedrock after smoothing the Fourier amplitude spectra by using Konno and Ohmachi algorithm with b=50 [77]. Figure A1 exhibits the amplification function *AF(f)* for the 9 parameter sets [37]. The fundamental resonance frequencies are close to the deterministic frequency, except for the higher COV (40%), for which a slightly lower frequency is obtained. The equivalent 1D deterministic model for the sediment layer over bedrock is then defined from the fundamental frequency $f_0$, determined from the first peak of the average amplification curve and

477 the average shear velocity ($\mu_{Vs}^{1D}$) computed as the logarithmic average of all *V*s values generated for the 100
478 realizations. The equivalent soil thickness *H* is then calculated using the relation $H = \mu_{Vs}^{1D}/4f_0$. The values of $f_0$ ,
479 $\mu_{Vs}^{1D}$ and *H* are given in Table A1 for all parameter sets.

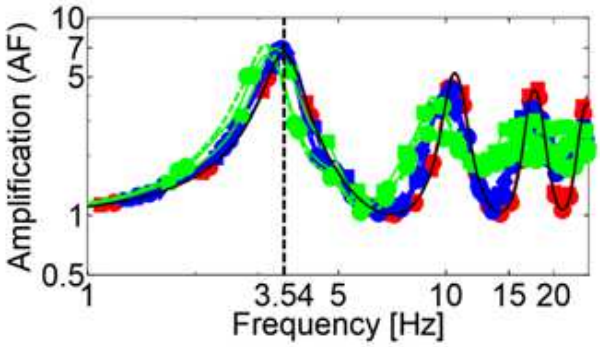


480

481 *Figure A1: Average outcrop amplification function at the central receiver (X=83 m) for*
482 *different values of COV, θx and θz computed using the 100 realizations. The black curve and*
483 *black dashed line refer to the amplification and the fundamental frequency of the*
484 *deterministic model, respectively [37].*

485

486 *Table A1: Properties of the 1D models equivalent to the 2D probabilistic models.*

| Parameter set # | Average shear-wave velocity $\mu_{Vs}^{1D}$ [m/s] | Fundamental frequency $f_0$ [Hz] | Equivalent soil thickness H $H$ [m] |
|---|---|---|---|
| **1** | 220 | 3.56 | 15.45 |
| **2** | 220 | 3.54 | 15.54 |
| **3** | 218 | 3.50 | 15.57 |
| **4** | 218 | 3.51 | 15.53 |
| **5** | 217 | 3.49 | 15.54 |
| **6** | 217 | 3.36 | 16.15 |
| **7** | 216 | 2.69 | 20.07 |
| **8** | 216 | 2.99 | 18.06 |
| **9** | 214 | 2.77 | 19.31 |

487

488

## Appendix 2: Vertical lagged coherency

The lagged coherency ($\gamma$) of the vertical component is calculated for all the parameter sets given in Table 1 and is shown in Figure 4 for 4 inter-receiver distances (from $d$ = 5 to 70 m). For small COV (5%) the coherency curves have the shape of a sinusoidal function, while for large COV (20% and 40%) the sinusoidal shape is attenuated with frequency. For all curves, the average coherency value decreases with the increase in *COV*. In contrast, the other parameters (autocorrelation distances) only exhibits slight influence on the coherency curves. The first maximum of the coherency curves is almost equal to the fundamental frequency of the deterministic model ($f_0 = 3.54\,Hz$) and the other maxima are at overtones ((n+3).$f_0$, for n=0, 1, 2…). As the seismic excitation is a pure SV wave at the base of the model, no vertical motion is expected at the surface. We interpret that S waves are scattered by the soil heterogeneities, distributing energy on the vertical component. The energy in the studied time window is then dominated by the vertical reverberation of the in-phase S-wave, leading to a maximum coherency at the resonance frequencies. Such sinusoidal shape is also observed on the lagged coherency calculated on the vertical surface velocity of the Koutavos-Argostoli recordings (Imtiaz et al., 2018a). However, for this case study, the first and second peaks are observed at 2 and 10 Hz, respectively, at almost $f_0$ and $5f_0$ of the site. No peak is observed at $3f_0$ (the resonant frequency of the third mode) and the observed oscillation periodicity (~8 Hz) does not correspond to the site fundamental frequency. Further research is needed to understand the origin of this oscillation and its relationship to the site characteristics.

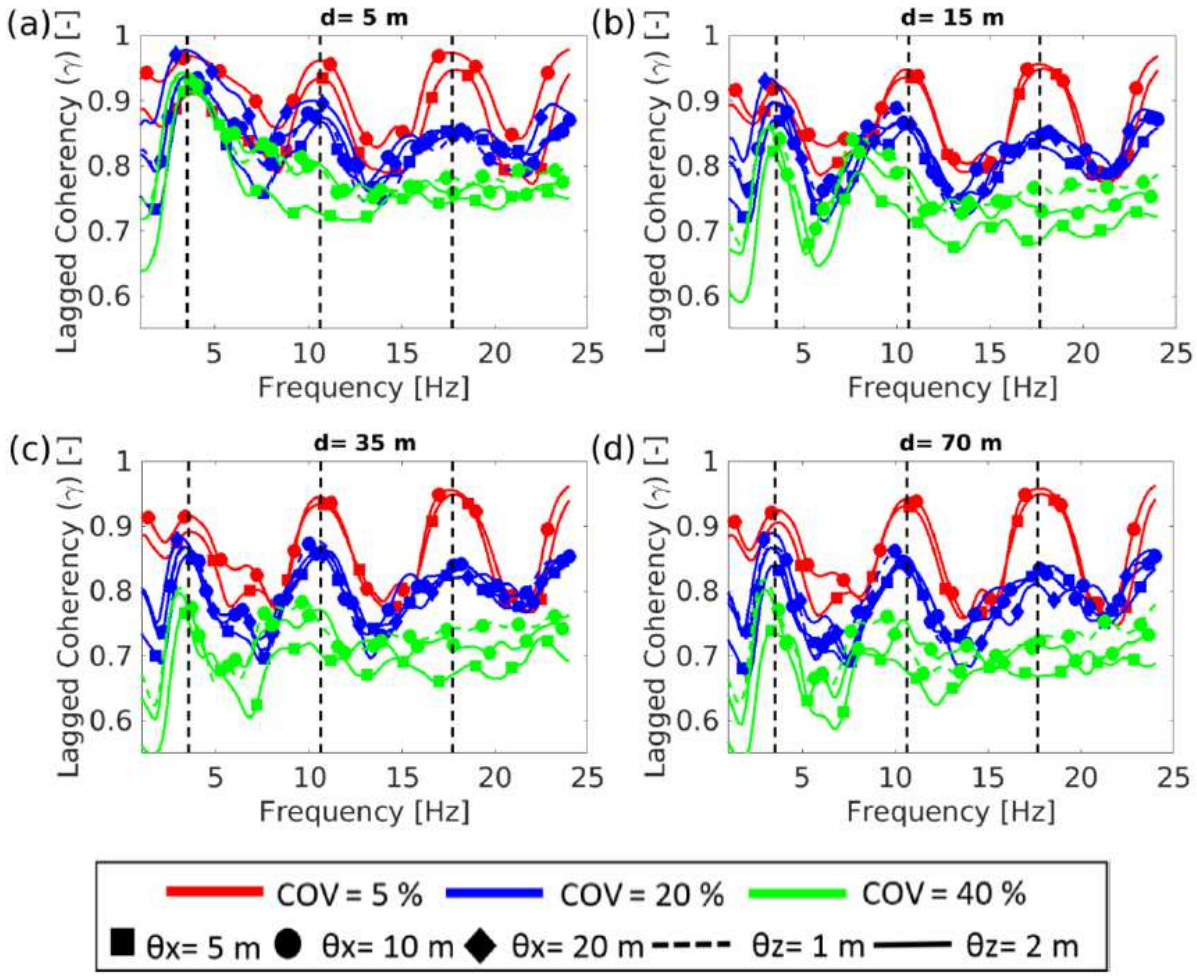


*Figure A2: Average lagged coherency (γ) calculated using the vertical component, for different values of COV, θx and θz for the 100 realizations computed by using the atanh transformation (see text for details) for four receivers distances: a) d = 5 m, b) d = 15 m, c) d = 35 m and d) d = 70 m. The resonant frequencies of the 3 fundamental modes of the deterministic model are indicated by black dashed vertical lines.*

## 9 Acknowledgments

This work was supported by Institut de Recherche pour le Développement (IRD), especially the ARTS doctoral thesis program, the IRD Young Research Unit JEAI SAMMOVA and GDRI O-LIFE.

## 10 References


[1] Hall, J. F., Holmes, W. T., & Somers, P. (1994). Northridge earthquake, January 17, 1994. Preliminary reconnaissance report.

[2] Chouw, N., & Hao, H. (2012). Pounding damage to buildings and bridges in the 22 February 2011 Christchurch earthquake. International Journal of Protective Structures, 3(2), 123-139.

[3] Shabestari, K. T., & Yamazaki, F. (2003). Near‐fault spatial variation in strong ground motion due to rupture directivity and hanging wall effects from the Chi‐Chi, Taiwan earthquake. Earthquake engineering & structural dynamics, 32(14), 2197-2219.

[4] Zerva, A., & Zervas, V. (2002). Spatial variation of seismic ground motions: an overview. Applied Mechanics Reviews, 55(3), 271-297.

[5] Der Kiureghian, A., & Neuenhofer, A. (1992). Response spectrum method for multi-support seismic excitations. Earthquake Engineering & Structural Dynamics, 21(8), 713-740.

[6] Zerva, A. (1992). Seismic loads predicted by spatial variability models. Structural Safety, 11(3-4), 227-243.

[7] Berrah, M. K., & Kausel, E. (1993). A modal combination rule for spatially varying seismic motions. Earthquake Engineering & Structural Dynamics, 22(9), 791-800.

[8] Der Kiureghian, A., Keshishian, P., & Hakobian, A. (1997). Multiple support response spectrum analysis of bridges including the site-response effect and the MSRS code (No. UCB/EERC-97/02).

[9] Saxena, V., Deodatis, G., & Shinozuka, M. (2000). Effect of spatial variation of earthquake ground motion on the nonlinear dynamic response of highway bridges. In Proc of 12th World Conf on Earthquake Engineering.

[10] Liao, S. (2006). Physical characterization of seismic ground motion spatial variation and conditional simulation for performance-based design.

[11] Hao, H., Oliveira, C. S., & Penzien, J. (1989). Multiple-station ground motion processing and simulation based on SMART-1 array data. Nuclear Engineering and Design, 111(3), 293-310.

[12] Somerville, P. G., McLaren, J. P., Sen, M. K., & Helmberger, D. V. (1991). The influence of site conditions on the spatial incoherence of ground motions. Structural Safety, 10(1-3), 1-13.

[13] Abrahamson, N. A. (1993, October). Spatial variation of multiple support inputs. In Proc of 1st US Seminar on Seismic Evaluation and Retrofit of Steel Bridges.

546 [14] Moczo, P., & Bard, P. Y. (1993). Wave diffraction, amplification and differential motion near strong
547 lateral discontinuities. Bulletin of the Seismological Society of America, 83(1), 85-106.
548 [15] Chávez-García, F. J., & Bard, P. Y. (1994). Site effects in Mexico City eight years after the September
549 1985 Michoacan earthquakes. Soil Dynamics and Earthquake Engineering, 13(4), 229-247.
550 [16] Field, E. H. (1996). Spectral amplification in a sediment-filled valley exhibiting clear basin-edge-
551 induced waves. Bulletin of the Seismological Society of America, 86(4), 991-1005.
552 [17] Graves, R. W., Pitarka, A., & Somerville, P. G. (1998). Ground-motion amplification in the Santa
553 Monica area: Effects of shallow basin-edge structure. Bulletin of the Seismological Society of America,
554 88(5), 1224-1242.
555 [18] Harichandran, R. S. (1999). Spatial variation of earthquake ground motion, what is it, how do we model
556 it, and what are its engineering implications. Dept. of Civil and Environmental Engineering, Michigan
557 State Univ., East Lansing, Mich.
558 [19] Jenny, H. (1941). Factors of soil formation: A system of quantitative pedology, 281 pp.
559 [20] Burrough, P. A. (1993). Soil variability revisited. Soils Fert, 56(5), 529-562.
560 [21] Lacasse, S., & Nadim, F. (1997). Uncertainties in characterising soil properties. Publikasjon-Norges
561 Geotekniske Institutt, 201, 49-75.
562 [22] Einsele, G. (2000). Sedimentary basins: evolution, facies, and sediment budget. Springer.
563 [23] Uzielli, M., Nadim, F., Lacasse, S., & Kaynia, A. M. (2008). A conceptual framework for quantitative
564 estimation of physical vulnerability to landslides. Engineering Geology, 102(3-4), 251-256.
565 [24] Pagliaroli, A., Lanzo, G., Tommasi, P., & Di Fiore, V. (2014b). Dynamic characterization of soils and
566 soft rocks of the Central Archeological Area of Rome. Bulletin of earthquake engineering , 12 (3),
567 1365-1381.
568 [25] Popescu, R. (1995). Stochastic variability of soil properties: data analysis, digital simulation, effects on
569 system behavior. Princeton University.
570 [26] Lopez-Caballero, Fernando, & Modaressi-Farahmand-Razavi, A. (2010). Assessment of variability and
571 uncertainties effects on the seismic response of a liquefiable soil profile. *Soil Dynamics and Earthquake*
572 *Engineering , 30* (7), 600-613.
573 [27] Youssef Abdel Massih, D. S., Soubra, A. H., & Mao, N. (2010). Reliability-based analysis of strip
574 footings subjected to an inclined or an eccentric loading. In GeoFlorida 2010: Advances in Analysis,
575 Modeling & Design (pp. 2133-2142).

576 [28] Al ‐ Bittar, T., & Soubra, A. H. (2014). Efficient sparse polynomial chaos expansion methodology for
577 the probabilistic analysis of computationally ‐ expensive deterministic models. International Journal for
578 Numerical and Analytical Methods in Geomechanics, 38(12), 1211-1230.
579 [29] Wang, S., & Hao, H. (2002). Effects of random variations of soil properties on site amplification of
580 seismic ground motions. Soil Dynamics and Earthquake Engineering, 22(7), 551-564.
581 [30] Sadouki, A., Harichane, Z., & Chehat, A. (2012). Response of a randomly inhomogeneous layered
582 media to harmonic excitations. Soil dynamics and earthquake engineering, 36, 84-95.
583 [31] Rodriguez ‐ Marek, A., Rathje, E. M., Bommer, J. J., Scherbaum, F., & Stafford, P. J. (2014).
584 Application of single-station sigma and site-response characterization in a probabilistic seismic-hazard
585 analysis for a new nuclear site. Bulletin of the Seismological Society of America, 104(4), 1601-1619.
586 [32] Berkane, H. D., Harichane, Z., Çelebi, E., & Elachachi, S. M. (2019). Site dependent and spatially
587 varying response spectra. Earthquake Engineering and Engineering Vibration, 18(3), 497-509.
588 [33] Assimaki, D., Pecker, A., Popescu, R., & Prevost, J. (2003). Effects of spatial variability of soil
589 properties on surface ground motion. Journal of earthquake engineering, 7(spec01), 1-44.
590 [34] Thompson, E., Baise, L., Kayen, R., & Guzina, B. (2009). Impediments to Predicting Site Response:
591 Seismic Property Estimation and Modeling Simplifications. Bulletin of the Seismological Society of
592 America, BSSA , 99, 2927-2949.
593 [35] Pagliaroli, A., Moscatelli, M., Raspa, G., & Naso, G. (2014a). Seismic microzonation of the central
594 archaeological area of Rome: results and uncertainties. Bull. Earthq. Eng. , 12, 1405–1428.
595 [36] Stripajova, S., Moczo, P., Kristek, J., Bard, P. Y., Hollender, F., & Sicilia, D. (2018). Extensive
596 numerical study on identification of key structural parameters responsible for site effects. In
597 Conference: 16th European Conference on Earthquake Engineering (16ECEE). At: Thessaloniki,
598 Greece.
599 [37] El Haber, E., Cornou, C., Jongmans, D., Abdelmassih, D. Y., Lopez-Caballero, F., & Al-Bittar, T.
600 (2019). Influence of 2D heterogeneous elastic soil properties on surface ground motion spatial
601 variability. Soil Dynamics and Earthquake Engineering, 123, 75-90.
602 [38] Abrahamson, N. A. (1990). Uncertainty in numerical strong motion predictions. In Proc. Fourth US
603 Nat. Conf. Earthq. Eng. (Vol. 1, pp. 407-416).

[39] Matsushima, Y. (1977). Stochastic response of structure due to spatially variant earthquake excitations. In Proceedings of Sixth World Conference on Earthquake Engineering (Vol. 2, pp. 1077-1082).

[40] Abrahamson, N., Schneider, J., & Stepp, J., 1990. Spatial variation of strong ground motion for use in soil structure interaction analyses, in Proceedings of the Fourth U.S. National Conference on Earthquake Engineering, Palm Springs, CA.

[41] Harichandran, R. S. (1991). Estimating the spatial variation of earthquake ground motion from dense array recordings. Structural Safety, 10(1-3), 219-233.

[42] Zerva, A. (2009). Spatial variation of seismic ground motion. Modeling and engineering applications.

[43] Abrahamson, N. A. (2007). Program on technology innovation: effects of spatial incoherence on seismic ground motions. EPRI, Palo Alto, CA, 1015110.

[44] Abrahamson, N. (1992). Spatial variation of earthquake ground motion for application to soil-structure interaction. Final report (No. EPRI-TR--100463-Tier1). Electric Power Research Inst., Palo Alto, CA (United States); Bechtel Civil, Inc., San Francisco, CA (United States); Woodward-Clyde Consultants, Pasadena, CA (United States).

[45] Harichandran, R. S., & Vanmarcke, E. H. (1986). Stochastic variation of earthquake ground motion in space and time. Journal of Engineering Mechanics, 112(2), 154-174.

[46] Ancheta, T., Stewart, J., & Abrahamson, N., 2011. Engineering characterization of earthquake ground motion coherency and amplitude variability, in Proc. 4th IASPEI / IAEE Int. Sym. on Effects of Surface Geology on Seismic Motion, pp. 23–26.

[47] Abrahamson, N. A. (2006). Program on technology innovation: spatial coherency models for soil-structure interaction. EPRI, Palo Alto, CA and the US Department of Energy: Report, 1012969.

[48] Luco, J. E., & Wong, H. L. (1986). Response of a rigid foundation to a spatially random ground motion. Earthquake Engineering & Structural Dynamics, 14(6), 891-908.

[49] Sato, H., Fehler, M. C., & Maeda, T. (2012). Seismic wave propagation and scattering in the heterogeneous earth (Vol. 496). Berlin: Springer.

[50] Svay, A. (2017). Modélisation de la variabilité spatiale du champ sismique pour les études d'interaction sol-structure. Phd thesis, Centrale Supelec, Paris.

[51] DeGroot, D. J. (1996). Analyzing spatial variability of in situ soil properties. In Uncertainty in the geologic environment: From theory to practice (pp. 210-238). ASCE.

[52] Phoon, K. K., & Kulhawy, F. H. (1999). Characterisation of geotechnical uncertainty. Canadian Geotechnical Journal, 36(4).

[53] Liu, C. N., & Chen, C. H. (2010). Spatial correlation structures of CPT data in a liquefaction site. Engineering Geology, 111(1-4), 43-50.

[54] Salloum, N. (2015). Evaluation de la variabilité spatiale des paramètres géotechniques du sol à partir de mesures géophysiques: application à la plaine alluviale de Nahr-Beyrouth (Liban). Phd thesis, Universite Joseph Fourier, Grenoble.

[55] Imtiaz, A., Perron, V., Svay, A., Hollender, F., Bard, P. Y., & Theodoulidis, N. (2017, January). Wavefield characteristics and coherency of seismic ground motion from a rocksite at Argostoli Greece. In Sixteenth World Conference on Earthquake Engineering (No. 1743).

[56] Vanmarcke, E. (2010). Random fields: analysis and synthesis. World Scientific.

[57] Der Kiureghian, A., & Ke, J. B. (1987). The stochastic finite element method in structural reliability. In Stochastic structural mechanics (pp. 84-109). Springer, Berlin, Heidelberg.

[58] Li, C.-C., & Der Kiureghian, A. (1993). Optimal discretization of random fields. *Journal of Engineering Mechanics , 119* (6), 1136-1154.

[59] Sacks, J., Welch, W. J., Mitchell, T. J., & Wynn, H. P. (1989). Design and analysis of computer experiments. Statistical science, 409-423.

[60] ITASCA. (2011). FLAC – Fast Lagrangian Analysis of Continua (Vol. Version 7.0). Minneapolis, USA: Itasca Consulting Group.

[61] Abrahamson, N. A., Schneider, J. F., & Stepp, J. C. (1991). Empirical spatial coherency functions for application to soil-structure interaction analyses. Earthquake spectra, 7(1), 1-27.

[62] Jenkins, G. M., & Watts, D. G. (1968). Spectral analysis.

[63] Imtiaz, A., Perron, V., Hollender, F., Bard, P. Y., Cornou, C., Svay, A., & Theodoulidis, N. (2018a). Wavefield Characteristics and Spatial Incoherency: A Comparative Study from Argostoli Rock - and Soil - Site Dense Seismic Arrays. Bulletin of the Seismological Society of America.

[64] Imtiaz, A., Cornou, C., & Bard, P. Y. (2018b). Sensitivity of ground motion coherency to the choice of time windows from a dense seismic array in Argostoli, Greece. Bulletin of Earthquake Engineering, 16(9), 3605-3625.

[65] Enochson, L. D., & Goodman, N. R. (1965). Gaussian approximations to the distribution of sample coherence (No. MAC-403-07). MEASUREMENT ANALYSIS CORP LOS ANGELES CA.

[66] Dziewonski, A., Bloch, S., & Landisman, M. (1969). A technique for the analysis of transient seismic signals. Bulletin of the seismological Society of America, 59(1), 427-444.

[67] Levshin, A., Ratnikova, L., & Berger, J. O. N. (1992). Peculiarities of surface-wave propagation across central Eurasia. Bulletin of the Seismological Society of America, 82(6), 2464-2493.

[68] Sheriff, R. E., & Geldart, L. P. (1995). Exploration seismology. Cambridge university press.

[69] Theodoulidis, N., Cultrera, G., Cornou, C., Bard, P. Y., Boxberger, T., DiGiulio, G., ... & Argostoli NERA Team. (2018a). Basin effects on ground motion: the case of a high-resolution experiment in Cephalonia (Greece). Bulletin of Earthquake Engineering, 16(2), 529-560.

[70] Theodoulidis, N., Hollender, F., Mariscal, A., Moiriat, D., Bard, P. Y., Konidaris, A., ... & Roumelioti, Z. (2018b). The ARGONET (Greece) Seismic Observatory: An Accelerometric Vertical Array and Its Data. Seismological Research Letters.

[71] Imtiaz, A. (2015). Seismic wave field, spatial variability and coherency of ground motion over short distances: near source and alluvial valley effects (Doctoral dissertation, Université Grenoble Alpes).

[72] Kanasewich, E. R. (1981). Time sequence analysis in geophysics. University of Alberta.

[73] Cranswick, E. (1988). The information content of high-frequency seismograms and the near-surface geologic structure of “hard rock” recording sites. In Scattering and Attenuations of Seismic Waves, Part I (pp. 333-363). Birkhäuser, Basel.

[74] Zerva, A., & Harada, T. (1997). Effect of surface layer stochasticity on seismic ground motion coherence and strain estimates. Soil Dynamics and Earthquake Engineering, 16(7-8), 445-457.

[75] Uscinski, B. J. (1977). The elements of wave propagation in random media. McGraw-Hill Companies.

[76] Gumbel, E. J. (1958). Statistical-theory of extreme values. Bull Internat Stat Inst, 36(3), 12-14.

[77] Konno, K., & Ohmachi, T. (1998). Ground-motion characteristics estimated from spectral ratio between horizontal and vertical components of microtremor. Bulletin of the Seismological Society of America, 88(1), 228-241.